

**Detection of the Ultraviolet Spectrum
of the Hot Subdwarf Companion of 60 Cygni (B1 Ve)
from a Survey of IUE Spectra of Be Stars**

Luqian Wang, Douglas R. Gies

*Center for High Angular Resolution Astronomy and Department of Physics and Astronomy,
Georgia State University, P. O. Box 5060, Atlanta, GA 30302-5060, USA*

lwang@chara.gsu.edu, gies@chara.gsu.edu

Geraldine J. Peters¹

*Space Sciences Center, University of Southern California, Los Angeles, CA 90089-1341,
USA*

gpeters@usc.edu

ABSTRACT

We used archival *International Ultraviolet Explorer* (*IUE*) high-dispersion, short wavelength spectra data to search for evidence of the spectra of hot subdwarf companions of six rapidly rotating Be stars in binary systems. We searched for the signature of a hot companion through an analysis of the cross-correlation functions of observed and model spectra that were separated into primary and secondary components using a Doppler tomography algorithm and adopted spectroscopic orbital solutions. A positive detection of the flux from a hot companion was made for the reconstructed secondary cross-correlation function of just one target, 60 Cygni (B1 Ve). We estimate that the companion of the Be star in 60 Cygni has $T_{\text{eff}} = 42 \pm 4$ kK, mass ratio $M_2/M_1 = 0.15 \pm 0.02$, and monochromatic flux ratio $f_2/f_1 = 0.034 \pm 0.002$ in the spectral region near 1525 Å. If the companions of the other target Be stars are also hot, then they must be faint and contribute less than $\approx 1\%$ of the UV flux ($< 0.6\%$ in the case of γ Cas). We also discuss in an appendix a shell episode of Pleione (28 Tau) recorded in the *IUE* spectra.

¹Guest Observer with the *International Ultraviolet Explorer*.

Subject headings: stars: emission-line, Be — stars: individual (γ Cas, 28 Tau, ζ Tau, κ Dra, 60 Cyg, π Aqr) — stars: binaries: spectroscopic — stars: evolution — stars: subdwarfs

1. Introduction

Be stars are B-type, main-sequence stars showing hydrogen emission features in their optical spectra (Rivinius et al. 2013). The Balmer line and excess continuum emission originates from a circumstellar disk that is inherently variable on time scales from days to centuries. Be stars are generally fast rotating objects, with equatorial rotating speeds of $> 70\%$ of their critical velocities. Their disks result from processes that are shedding the stellar angular momentum, and disk formation episodes may be linked to pulsational mode beating in some Be stars (e.g., η Cen and μ Cen; Baade et al. 2016).

The cause of the rapid rotation of Be stars is due in some cases to past mass transfer in interacting binary systems (Pols et al. 1991; Shao & Li 2014). Roche lobe overflow of the initially more massive, mass donor star will lead to spin-up of the gainer and an increase in orbital period once mass ratio reversal occurs. The final stripped-down donor star may explode to create a Be star – neutron star X-ray binary, or, if the remnant is below the Chandrasekhar mass limit, the binary system will consist of a Be star with a faint low-mass white dwarf or helium subdwarf star (sdO). Detection of such subdwarf companions is difficult because they are relatively faint and their low mass creates only small orbital motions in the Be star companions.

Nevertheless, we have now detected the flux of subdwarf companions in four systems. The search is best made at short wavelengths because the subdwarfs are usually hotter than their Be star companions and thus contribute relatively more flux in the ultraviolet (UV). The first direct spectroscopic detection of a sdO companion in the Be system ϕ Per was accomplished with UV spectra from the *International Ultraviolet Explorer (IUE)* (Thaller et al. 1995), and the binary properties were established through *Hubble Space Telescope* UV spectroscopy (Gies et al. 1998) and optical interferometry (Mourard et al. 2015). Subsequently, Peters et al. (2008) and Peters et al. (2013) applied similar search techniques with *IUE* to detect subdwarf companions in the Be binaries FY CMa and 59 Cyg, respectively. Finally, the flux of a relatively very faint companion was detected by Peters et al. (2016) from a large set of *IUE* spectra of HR 2142. The gravitational pull of the companion creates a tidal wake in the disk of the Be star in HR 2142 that leads to the appearance of “shell lines” (narrow absorption features) when the subdwarf is in the foreground. These four Be+sdO binaries may be related to recently discovered systems consisting of an intermediate mass,

main-sequence star and a hot, low mass white dwarf that was stripped of its envelope by binary mass transfer (Maxted et al. 2014; Matson et al. 2015; Rappaport et al. 2015). We note for completeness that there are three known late B-type plus white dwarf systems (detected through their flux in the extreme ultraviolet; Vennes et al. 1997; Burleigh & Barstow 1998, 1999), but these are thought to be non-interacting systems in which the white dwarf formed by a single-star evolutionary route.

Based on the positive detection of companions in these four Be systems, here we expand the search for subdwarfs in another six Be binary systems that were observed many times over the lifetime of *IUE*. All of these targets are known single-lined spectroscopic binaries with hitherto undetected, low mass companions. The targets are listed in Table 1 with spectral classifications from Slettebak (1982) and projected rotational velocities from Frémat et al. (2005). We briefly summarize below the key studies on their orbital and physical properties.

γ Cas (HD 5394). This is the first spectroscopically observed Be star by Secchi (1866). The binarity of the system was confirmed by Nemravová et al. (2012) through a 16.84 year span of optical spectra monitoring. Extensive studies of the star’s X-ray emission and circumstellar environment (Smith et al. 2012; Stee et al. 2012; Hamaguchi et al. 2016) suggest that the X-ray emission is associated with parts of the disk gas of the Be star, so that the companion need not be an accreting neutron star or white dwarf. Several other X-ray emitting Be stars like γ Cas appear to be “blue stragglers” that may have been formed through binary mass transfer (Smith et al. 2016).

28 Tau (HD 23862). Pleione is a known shell star with cyclic variability lasting decades. The shell activity that occurred over the duration of the *IUE* observations is discussed in the Appendix. Nemravová et al. (2010) confirmed it as the primary component of the binary system through Doppler shifts from $H\alpha$ emission spectroscopy.

ζ Tau (HD 37202). Hynek & Struve (1942) confirmed the binarity of the system using radial velocities from Balmer lines measured in photographic plates, and Delplace (1971) estimated the system dimensions by considering the size of the Be disk. Ruždjak et al. (2009) improved the orbital ephemeris of the system from $H\alpha$ spectroscopy and *UBV* photometry observations over about a century.

κ Dra (HD 109387). Saad et al. (2005) determined the orbit of the binary through wide-ranging spectroscopic observations. They found no direct evidence of the companion’s spectrum.

60 Cyg (HD 200310). Plaskett & Pearce (1931) reported that the star belongs to a spectroscopic binary system. Koubský et al. (2000) discussed the long, medium, and short term variability in the observed spectra and light curves, and they presented orbital elements from radial velocity measurements of the Be star.

π Aqr (HD 212571). Bjorkman et al. (2002) discovered the binary nature through a radial

velocity analysis of the absorption and emission lines. They suggested that the companion could be an A- or F-type main-sequence star, but the absorption spectrum of the companion was not observed. Zharikov et al. (2013) made an analysis of the orbital variations of the H α emission line. They estimated that the secondary has a mass $< 2M_{\odot}$.

Here we present results of our analysis of the UV spectra from *IUE* to search for subdwarf companions of these six systems. Section 2 presents our subdwarf flux search method that is based upon a cross-correlation analysis of the UV spectra with model spectral templates for the subdwarf spectra. Our results are discussed in Section 3.

2. Search for the UV Flux of Hot Companions

Our search technique is centered on forming a cross-correlation function (CCF) of the observed spectra with model spectra for the expected effective temperature T_{eff} of a hot companion. Two issues make this process difficult. First, any companion is probably relatively faint compared to its Be host star, so given the low S/N of the *IUE* spectra (≈ 20 per resolution element; Nichols & Linsky 1996), it will be hard to identify the signal of the companion in the CCF for any one spectrum. Second, some of the lines in the model spectrum of the hot companion may also be present (although weaker) in the spectrum of the Be star, so the derived CCF may present a composite of companion and Be signals. Our solution here is to apply a Doppler tomography algorithm (Bagnuolo et al. 1994) to the derived CCFs in order to separate both the companion and Be star CCF components and to use all the spectra together to increase the net S/N of the reconstructed CCFs. Below we outline how the spectra are organized, how the trial velocity curves were estimated for the components, and details of the CCF reconstruction process. The final results for the reconstructed secondary CCFs are discussed at the end of the section and are shown in Figure 1.

We downloaded the high dispersion, short wavelength prime (SWP) spectra of the selected targets from MAST². The number of available spectra and their time span are listed in Table 1. The spectra have a resolving power of $\lambda/\Delta\lambda = 13,000$, and the wavelength coverage is from 1150 Å to 1950 Å. The individual echelle orders were merged and placed on a heliocentric grid using the standard *IUE* IDL data reduction pipeline *iuerdaf*. The spectra were then transformed onto a uniform heliocentric wavelength grid in $\log \lambda$ steps equivalent to 10 km s⁻¹, and for the more distant stars (HD 5394, HD 200310, and HD 212571 with $d > 180$ pc), the wavelength calibration was checked through alignment (and then removal) of interstellar lines. The spectra were rectified with respect to the relatively

²<https://archive.stsci.edu/iue/>

line-free parts of the spectra into a final matrix of stellar flux as a function of wavelength and time of observation.

The next aspect of the process was to estimate the radial velocities of both components at the time of observation. We initially measured radial velocities of the Be components using the CCF methods adopted in past work (Peters et al. 2016), but the scatter in the results (and poor phase coverage in some cases) was too large to offer any improvement over the existing orbital solutions. Consequently we adopted the published orbital elements for the Be star primaries that are summarized in Table 2. Then we calculated velocities for the primary Be star at the times of observation using these solutions. The secondary star velocities were derived from the primary velocities using the systemic velocity γ and an assumed mass ratio $q = M_2/M_1$. This mass ratio was calculated from the spectroscopic mass function and published estimates of the Be star mass and system inclination. The latter two parameters were taken from Silaj et al. (2014) and the references cited in Table 2. The derived values of q are given in column 8 of Table 2.

Each spectrum was cross-correlated with a model spectrum that was derived from the grid of synthetic spectra for hot stars using the non-local thermal equilibrium (non-LTE) atmosphere program TLUSTY and the associated radiative transfer code SYNSPEC from Lanz & Hubeny (2003). The default model temperature was set to $T_{\text{eff}} = 45$ kK, a value similar to that found for other hot subdwarf systems (Peters et al. 2016), and the gravity was assigned a value of $\log g = 4.75$, the highest gravity available in the grid but probably lower than expected. The model spectrum is based upon a solar abundance and a microturbulent velocity of 10 km s^{-1} . The synthetic spectrum was rectified to a unit continuum, rebinned onto the observed $\log \lambda$ grid, and smoothed to the instrumental broadening of $\text{FWHM} = 25 \text{ km s}^{-1}$. No rotational broadening was applied given the sharp appearance of the subdwarf spectra in other Be binary systems. We excluded the beginning and ending regions, plus very broad wind lines from the spectra before calculating the CCF to avoid introduction of troublesome wide structures in the CCF. The regions adjoining the excluded zones were gradually smoothed to a pure continuum using a Tukey filter function, which applies a cosine function to reduce line depths close to the boundaries. The final result is an array of CCF functions corresponding to each observed spectrum.

The derived CCF functions usually display a wide and shallow peak because of some correlation between the broad lines of the Be star spectrum and the model spectrum. We suppose that each CCF is the sum of a broad component from the Be star and a possible narrow component from the subdwarf star, each Doppler-shifted accord to the orbital velocity at the time of observation. Then we performed a reconstruction of these two components using the Doppler tomography algorithm of Bagnuolo et al. (1994). This procedure assumes

radial velocity shifts from the adopted orbital elements (Table 2), and then uses an iterative scheme to reconstruct the two components that when shifted and co-added make the best fit of the observed CCFs. In this instance, we assumed that both components contribute equally to the combined CCF, and consequently we divided the results by a factor of two so that the CCF amplitude matches that in the observed CCFs. The iterative scheme begins by assuming that the primary CCF is equal to the simple mean of all the CCFs and that the secondary CCF is flat and featureless (no secondary signal is present).

The reconstructed primary component appears almost flat in the cases of the cooler Be star primaries (28 Tau and κ Dra) because there is very little correlation between the features in their and the model spectra. However, the primary CCFs for the hotter Be stars (γ Cas, ζ Tau, 60 Cyg, π Aqr) are broad as expected for the broad and shallow absorption lines in their spectra that are common to those in the hot model spectrum. The trial reconstructed CCFs for the secondaries are generally shallow with some low frequency curvature due to the characteristics of the spectral rectification and line clusters. In order to remove the variations in the background, we first smoothed the secondary CCF by convolution with a Gaussian of $\text{FWHM} = 350 \text{ km s}^{-1}$, and then we subtracted this smoothed background variation from the secondary CCF to search for any narrow peak associated with a hot subdwarf spectral component. The resulting secondary CCFs are plotted in Figure 1, and they generally appear featureless, with the striking exception of 60 Cyg, in which we see a prominent peak near the expected zero velocity in the frame of reference of the secondary star. Thus, our search method has led to the discovery of one new detection of a hot companion to the Be star 60 Cyg. In the next section, we discuss the properties of the companion of 60 Cyg and consider the flux limits of the companions of the other five targets.

3. Discussion

The detection of the spectral signature of the hot companion of 60 Cyg involved making assumptions about the mass ratio and companion effective temperature. We next explore how changing these parameters can help us find better estimates of their values. We began by repeating the analysis for a grid of assumed mass ratios, and in each case we fit a Gaussian to the peak in the reconstructed secondary CCF. The CCF peak attains a maximum at $q = M_2/M_1 = 0.146 \pm 0.023$, where the uncertainty represents the half-range of mass ratios where the peak height is within the 1σ zone of the maximum CCF peak height of 0.0335 ± 0.0015 . We note that this estimate of the mass ratio is the same within uncertainties as the trial mass ratio we derived from the primary mass function, mass, and system inclination (Table 1). We fixed the mass ratio to this result, and then repeated the analysis using TLUSTY/SYNSPEC

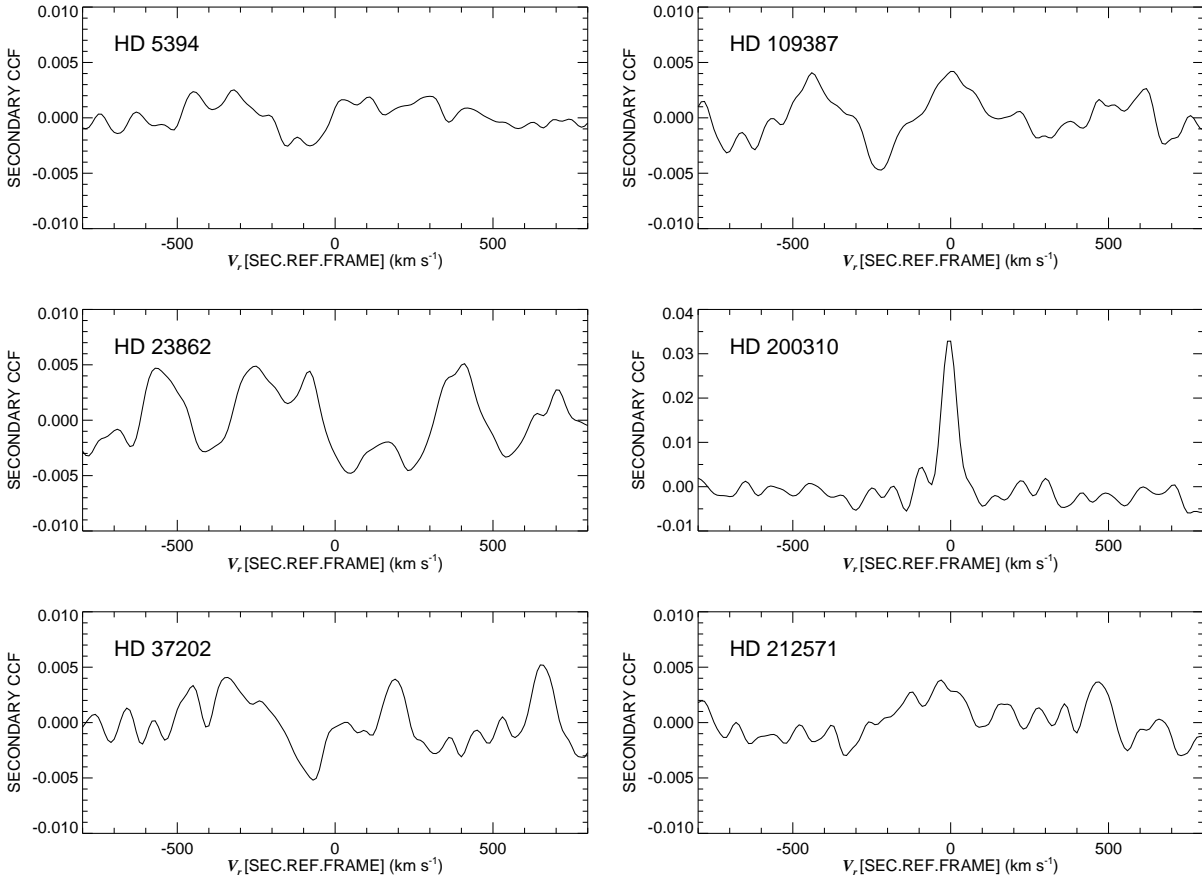


Fig. 1.— The reconstructed secondary CCFs of the six Be binary systems derived from the assumed Doppler shifts of the secondary and a model hot reference spectrum ($T_{\text{eff}} = 45$ kK). A detected peak is only seen in the case of 60 Cyg = HD 200310.

model spectra for the cross-correlation template that ranged from $T_{\text{eff}} = 27.5$ to 55 kK. We made a spline fit of peak height as a function of assumed temperature to arrive at an estimate of $T_{\text{eff}} = (42 \pm 4)$ kK for the companion.

We are also interested in determining the UV flux ratio that would produce a secondary CCF with the observed peak height. We determined this quantity by first creating a subdwarf model spectrum for $T_{\text{eff}} = 42$ kK, $\log g = 4.75$, $V \sin i = 0$, and constructing a Be star model for $T_{\text{eff}} = 27$ kK, $\log g = 4.0$, $V \sin i = 320$ km s⁻¹ (Koubský et al. 2000). Then we created a model set of observations over an assumed grid of flux ratios in the following way. For each time of observation, the model spectra were shifted by the assigned orbital Doppler velocities. Next the model secondary spectrum was rescaled in flux to match that of the

model primary spectrum in the range 1500 – 1550 Å. Then the model secondary spectrum was rescaled again in flux according to the assumed monochromatic flux ratio f_2/f_1 . The sum of the model primary and rescaled secondary spectra was then rectified to a unit continuum. We then repeated the CCF and tomography analysis of this model set of spectra in the same way as done with the observed spectra to derive a relationship between reconstructed secondary CCF peak height and the assumed flux ratio f_2/f_1 at 1525 Å. Interpolating the observed CCF peak height in this relation led to a monochromatic flux ratio estimate of $f_2/f_1 = 0.0339 \pm 0.0015$ at 1525 Å. This flux ratio is related to the ratio of stellar radii by

$$\frac{f_2}{f_1} = \frac{F_2}{F_1} \times \left(\frac{R_2}{R_1}\right)^2 \quad (1)$$

where F_2/F_1 is the monochromatic surface flux ratio of the stars and is equal to $F_2/F_1 = 3.88$ in the continuum at 1525 Å for the adopted temperatures of the two stars in the TLUSTY models. Using the above relation, the resulting radius ratio is $\frac{R_2}{R_1} = 0.093 \pm 0.012$, where the uncertainty includes the range of F_2/F_1 associated with the error in T_{eff} .

Koubský et al. (2000) estimate that the Be star mass and mean radius of 60 Cyg are $M_1 = 11.8M_\odot$ and $R_1 = 5.1R_\odot$, respectively. If we adopt these values, then the mass, radius, and gravity of the subdwarf are $M_2 = 1.7M_\odot$, $R_2 = 0.48R_\odot$, and $\log g_2 = 5.3$, respectively. This estimate of the companion mass places it above the Chandrasekhar limit of $1.4M_\odot$, so it is possible that the subdwarf may become a neutron star in the future. If so, then 60 Cyg may be a progenitor of a Be X-ray binary system. The estimated gravity of the subdwarf is higher than the limit in the TLUSTY grid $\log g = 4.75$ that we used in deriving the best fit T_{eff} . The relative strengths of the spectral features in the model spectra depend on the ionization balance in the model, so if we had used a higher $\log g$ model, we would probably arrive at a slightly higher estimate of T_{eff} and a somewhat lower value of R_2 .

It is remarkable that among the now five known Be+subdwarf systems that 60 Cyg and 59 Cyg are separated by about one degree on the sky. The stars are not known as cluster members, but they may be affiliated with other early-type stars in their vicinity. We formed a list of stars with B spectral classifications within 2° of the midpoint between 59 Cyg and 60 Cyg from the catalog of Skiff (2014), and then collected proper motions from the Gaia Collaboration (2016) and parallaxes from van Leeuwen (2007) for these stars. Table 3 shows those selected with proper motions and parallaxes within 2σ of those of 59 Cyg (HD 200120) and 60 Cyg (HD 200310). This collection of six objects may form part of a hitherto unknown co-moving group of equal age stars. If so, then 59 Cyg and 60 Cyg may be at a similar stage of binary evolution because of their common origin and age.

We found no evidence of the companion flux in the other five Be binaries. We placed a constraint on the relative flux of the undetected companion in the same way as we found the

flux ratio for 60 Cyg by creating model observation sets for the adopted stellar parameters and then finding the relation between f_2/f_1 at 1525 Å and the secondary CCF peak height. We used these relations and the observed standard deviations in the derived CCFs (Fig. 1) to estimate a conservative upper limit on f_2/f_1 that would yield a 5σ peak in the CCF. These limits on the monochromatic flux are listed in column 9 of Table 2, and in general they indicate that the companions contribute no more than 1% of the flux at 1525 Å. We caution that these limits tacitly assume that the companions are hot and narrow-lined, which may not be correct in all cases. Nevertheless, the results suggest that if the companions are hot, then they must have small radii and relatively low luminosity. For example, the flux ratio limit is the smallest in the case of γ Cas, $f_2/f_1 < 0.006$, and this limit implies $R_2/R_\odot < 0.3$ and $\log L_2/L_\odot < 2.6$. The faintness of such companions is probably consistent with evolutionary models that predict that such post-mass transfer remnants spend most of their remaining He-burning lifetime as faint, core He-burning objects (A. Schootemeijer et al. 2017, in preparation).

The data presented in this paper were obtained from the Mikulski Archive for Space Telescopes (MAST). STScI is operated by the Association of Universities for Research in Astronomy, Inc., under NASA contract NAS5-26555. Support for MAST for non-HST data is provided by the NASA Office of Space Science via grant NNX09AF08G and by other grants and contracts. Our work was supported in part by NASA grant NNX10AD60G (GJP) and by the National Science Foundation under grant AST-1411654 (DRG). Institutional support has been provided from the GSU College of Arts and Sciences, the Research Program Enhancement fund of the Board of Regents of the University System of Georgia (administered through the GSU Office of the Vice President for Research and Economic Development), and by the USC Women in Science and Engineering (WiSE) program (GJP). This work has made use of data from the European Space Agency (ESA) mission *Gaia*, processed by the *Gaia* Data Processing and Analysis Consortium (DPAC). Funding for the DPAC has been provided by national institutions, in particular the institutions participating in the *Gaia* Multilateral Agreement.

Facilities: IUE

A. Shell Episode of Pleione

Pleione shows long term variations in brightness and color during the B, Be, and Be-shell phase transitions. During a shell phase the optical spectrum of hydrogen and metallic lines show narrow absorption cores with significant growth in line strength, and these spectral variations probably result from physical changes in the circumstellar disk as projected against the photosphere of the star. Cramer et al. (1995) summarized the light variations of Pleione from 1880 to 1993 through optical photometry, and they documented how the B -magnitude of Pleione changed during the shell episode from 1973 to 1993. A significant drop in brightness occurred prior to the shell phase in 1973, and then the star’s brightness gradually increased as the shell lines faded and Pleione returned to the Be phase. Doazan et al. (1988) investigated the spectral variability of the metallic lines in far-UV during this time, and Doazan et al. (1993) showed how the energy flux between 1250 and 3000 Å varied from 1979 to 1991.

The full set of *IUE* spectra record the shell line changes from 1979 to 1995, and we plot the average flux of Pleione in the UV from 1160 to 1450 Å in Figure 2 (top panel). The average UV flux dropped significantly after 1979, reached a minimum in 1982, and then slowly increased back to the average level. The three low flux measurements (1980 – 1982) were recorded through the small aperture of the camera, which may underestimate the actual flux. Nevertheless, a similar local minimum was also recorded at the same time in the B -band photometry from Cramer et al. (1995). There are shell lines in the UV spectra that are very narrow and that are also observed in cooler objects like A-type stars. Thus, we measured the strength of shell lines of Pleione by calculating CCFs with a star that has a line spectrum similar to the shell features. We adopted the supergiant star HD 197345 (Deneb, A2Ia) to cross-correlate with the spectrum of Pleione, and shell line regions including 1450 – 1500 Å, 1510 – 1583 Å, 1650 – 1700 Å, and 1828 – 1875 Å were chosen to calculate the CCFs. In Figure 2, the middle panel shows how the shell line strength decreased as the star brightened. We also calculated the relative radial velocity of the shell lines from the peak position of CCFs with the Deneb spectrum. Parthasarathy & Lambert (1987) reported that Deneb has a mean radial velocity of -13.67 km s^{-1} , so we added this velocity to the CCF relative velocities to obtain the absolute radial velocities of the shell lines that are plotted in bottom panel of Figure 2. The shell line velocities appear to become more negative relative to Pleione (systemic velocity of -0.15 km s^{-1} from Nemravová et al. 2010) as the shell episode declines. However, near the final stage of the shell episode, the CCFs are weak, so the measured velocities have large uncertainties. Our results are consistent with those reported by Underhill & Doazan (1982) in their Figure 11–43, which show that the velocities have greatest expansion at the epoch of shell line disappearance. The shell line spectra show significant blue-shifts during the Be-shell to Be phase transition, and the negative velocities

suggest that the opaque gas associated with the shell lines moves away from the star as the shell episode concludes.

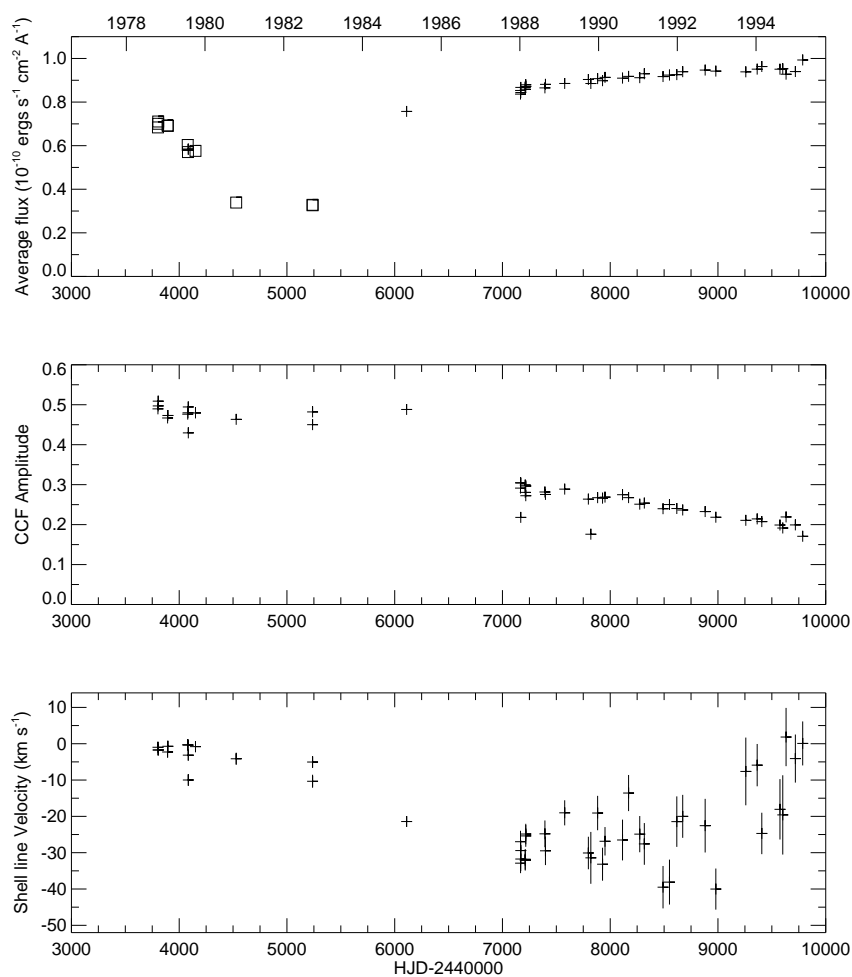


Fig. 2.— The shell line variations of Pleione in UV from 1979 to 1995. *Top panel:* the average flux is computed in the wavelength region [1160, 1450] \AA ; spectra recorded in large and small apertures are denoted as crosses and squares, respectively. *Middle panel:* cross-correlation strength between the spectra of Pleione and supergiant star Deneb. *Bottom panel:* absolute radial velocities from the cross-correlation functions of the shell lines.

REFERENCES

- Baade, D., Rivinius, T., Pigulski, A., et al. 2016, *A&A*, 588, A56
- Bagnuolo, Jr., W. G., Gies, D. R., Hahula, M. E., Wiemker, R., & Wiggs, M. S. 1994, *ApJ*, 423, 446
- Bjorkman, K. S., Miroshnichenko, A. S., McDavid, D., & Pogrosheva, T. M. 2002, *ApJ*, 573, 812
- Burleigh, M. R., & Barstow, M. A. 1998, *MNRAS*, 295, L15
- . 1999, *A&A*, 341, 795
- Cramer, N., Doazan, V., Nicolet, B., de La Fuente, A., & Barylak, M. 1995, *A&A*, 301, 811
- Delplace, A. M. 1971, *A&A*, 10, 246
- Doazan, V., Bourdonneau, B., & Thomas, R. N. 1988, *A&A*, 205, L11
- Doazan, V., de La Fuente, A., Barylak, M., Cramer, N., & Mauron, N. 1993, *A&A*, 269, 415
- Frémat, Y., Zorec, J., Hubert, A.-M., & Floquet, M. 2005, *A&A*, 440, 305
- Gaia Collaboration. 2016, *VizieR Online Data Catalog*, 1337
- Gies, D. R., Bagnuolo, Jr., W. G., Ferrara, E. C., et al. 1998, *ApJ*, 493, 440
- Hamaguchi, K., Oskinova, L., Russell, C. M. P., et al. 2016, *ApJ*, 832, 140
- Hynek, J. A., & Struve, O. 1942, *ApJ*, 96, 425
- Koubský, P., Harmanec, P., Hubert, A. M., et al. 2000, *A&A*, 356, 913
- Lanz, T., & Hubeny, I. 2003, *ApJS*, 146, 417
- Matson, R. A., Gies, D. R., Guo, Z., et al. 2015, *ApJ*, 806, 155
- Maxted, P. F. L., Bloemen, S., Heber, U., et al. 2014, *MNRAS*, 437, 1681
- Mourard, D., Monnier, J. D., Meilland, A., et al. 2015, *A&A*, 577, A51
- Nemravová, J., Harmanec, P., Kubát, J., et al. 2010, *A&A*, 516, A80
- Nemravová, J., Harmanec, P., Koubský, P., et al. 2012, *A&A*, 537, A59
- Nichols, J. S., & Linsky, J. L. 1996, *AJ*, 111, 517

- Parthasarathy, M., & Lambert, D. L. 1987, *Journal of Astrophysics and Astronomy*, 8, 51
- Peters, G. J., Gies, D. R., Grundstrom, E. D., & McSwain, M. V. 2008, *ApJ*, 686, 1280
- Peters, G. J., Pewett, T. D., Gies, D. R., Touhami, Y. N., & Grundstrom, E. D. 2013, *ApJ*, 765, 2
- Peters, G. J., Wang, L., Gies, D. R., & Grundstrom, E. D. 2016, *ApJ*, 828, 47
- Plaskett, J. S., & Pearce, J. A. 1931, *Publications of the Dominion Astrophysical Observatory Victoria*, 5, 1
- Pols, O. R., Cote, J., Waters, L. B. F. M., & Heise, J. 1991, *A&A*, 241, 419
- Rappaport, S., Nelson, L., Levine, A., et al. 2015, *ApJ*, 803, 82
- Rivinius, T., Carciofi, A. C., & Martayan, C. 2013, *A&A Rev.*, 21, 69
- Ruždjak, D., Božić, H., Harmanec, P., et al. 2009, *A&A*, 506, 1319
- Saad, S. M., Kubát, J., Hadrava, P., et al. 2005, *Ap&SS*, 296, 173
- Secchi, A. 1866, *Astronomische Nachrichten*, 68, 63
- Shao, Y., & Li, X.-D. 2014, *ApJ*, 796, 37
- Silaj, J., Jones, C. E., Sigut, T. A. A., & Tycner, C. 2014, *ApJ*, 795, 82
- Skiff, B. A. 2014, *VizieR Online Data Catalog*, 1
- Slettebak, A. 1982, *ApJS*, 50, 55
- Smith, M. A., Lopes de Oliveira, R., & Motch, C. 2016, *Advances in Space Research*, 58, 782
- Smith, M. A., Lopes de Oliveira, R., Motch, C., et al. 2012, *A&A*, 540, A53
- Stee, P., Delaa, O., Monnier, J. D., et al. 2012, *A&A*, 545, A59
- Thaller, M. L., Bagnuolo, Jr., W. G., Gies, D. R., & Penny, L. R. 1995, *ApJ*, 448, 878
- Underhill, A., & Doazan, V. 1982, *B Stars with and without emission lines (NASA SP-456)*
- van Leeuwen, F. 2007, *A&A*, 474, 653
- Vennes, S., Berghöfer, T. W., & Christian, D. J. 1997, *ApJ*, 491, L85

Zharikov, S. V., Miroshnichenko, A. S., Pollmann, E., et al. 2013, *A&A*, 560, A30

Table 1. *IUE* Observations of Be Binary Systems

Star Name	HD Number	HIP Number	Spectral Classification	$V \sin i$ (km s^{-1})	Number of Observations	Time span (years)
γ Cas	5394	4427	B0.5 IVe	432	228	18
28 Tau	23862	17851	B8 Ve shell	286	48	17
ζ Tau	37202	26451	B1 IVe shell	310	34	17
κ Dra	109387	61281	B5 IIIe	200	26	11
60 Cyg	200310	103732	B1 Ve	300	23	15
π Aqr	212571	110672	B1 III-IVe	230	22	17

Note. — Spectral classifications and projected rotational velocities are from Slettebak (1982) and Frémat et al. (2005), respectively.

Table 2. Adopted Orbital Elements

HD Number	P (days)	T^a (HJD-2,400,000)	e	ω (deg)	K_1 (km s ⁻¹)	γ (km s ⁻¹)	Trial M_2/M_1	f_2/f_1	Source Reference
5394	203.523 ± 0.076	52183.65 ± 0.62	0.0	...	4.30 ± 0.09	0.02 ± 0.06	0.072	< 0.006	Nemravová et al. (2012)
23862	218.023 ± 0.023	40040.4 ± 1.6	0.596 ± 0.035	147.7 ± 4.5	5.41 ± 0.35	-0.15 ± 0.1	0.082	< 0.026	Nemravová et al. (2010)
37202	132.987 ± 0.050	47025.6 ± 1.8	0.0	...	7.43 ± 0.46	20.0 ± 0.4	0.084	< 0.013	Ruždjak et al. (2009)
109387	61.555 ± 0.029	49980.22 ± 0.59	0.0	...	6.81 ± 0.24	...	0.114	< 0.010	Saad et al. (2005)
200310	146.6 ± 0.6	50016.9 ± 1.9	0.0	...	10.8 ± 0.1	-13.4	0.131	0.034	Koubský et al. (2000)
212571	84.135 ± 0.004	50316.91 ± 0.04	0.0	...	16.7 ± 0.2	-4.9 ± 0.1	0.163	< 0.010	Bjorkman et al. (2002)

^aFor systems with circular orbits, the epoch corresponds to the time of Be star maximum radial velocity, and for the eccentric orbit of HD 23682, the epoch corresponds to the time of periastron.

Table 3. Co-moving Stars in the Vicinity of 59 Cyg and 60 Cyg

HD Number	V (mag)	Spectral Classification	μ_α (mas y ⁻¹)	μ_δ (mas y ⁻¹)	π (mas)	V_r (km s ⁻¹)
198625	6.33	B4 Ve	4.2 ± 1.0	3.8 ± 1.0	2.03 ± 0.34	–15
199309	8.65	B8 V	6.4 ± 0.6	2.6 ± 0.6	3.08 ± 0.70	–25
199889	8.33	B8 V	6.4 ± 0.6	3.1 ± 0.6	3.10 ± 0.52	–22
200120	4.75	B1.5 Vne	7.3 ± 1.0	2.5 ± 1.0	2.30 ± 0.42	–10
200310	5.43	B1.5 IV-Vne	6.1 ± 1.0	3.4 ± 1.0	2.14 ± 0.37	–13
200615	8.13	B8 V	6.0 ± 0.7	1.4 ± 0.6	1.69 ± 0.53	–17

Note. — The spectral classifications are from the collection by Skiff (2014), proper motions μ_α and μ_δ are from the Gaia Collaboration (2016), and parallaxes are from van Leeuwen (2007). The V magnitude and radial velocity data are from SIMBAD, with the exception of the systemic velocities for 59 Cyg (Peters et al. 2013) and 60 Cyg (Koubský et al. 2000).